scientific reports

Check for updates

OPEN

The crystal structure of *Acinetobacter baumannii* bacterioferritin reveals a heteropolymer of bacterioferritin and ferritin subunits

Huili Yao[1], Suliat Alli[1], Lijun Liu[2], Anabel Soldano[1], Anne Cooper[2], Leo Fontenot[1], Dristen Verdin[1], Kevin P. Battaile[3], Scott Lovell[2]✉ & Mario Rivera[1]✉

Iron storage proteins, e.g., vertebrate ferritin, and the ferritin-like bacterioferritin (Bfr) and bacterial ferritin (Ftn), are spherical, hollow proteins that catalyze the oxidation of Fe^{2+} at binuclear iron ferroxidase centers (FOC) and store the Fe^{3+} in their interior, thus protecting cells from unwanted Fe^{3+}/Fe^{2+} redox cycling and storing iron at concentrations far above the solubility of Fe^{3+}. Vertebrate ferritins are heteropolymers of H and L subunits with only the H subunits having FOC. Bfr and Ftn were thought to coexist in bacteria as homopolymers, but recent evidence indicates these molecules are heteropolymers assembled from Bfr and Ftn subunits. Despite the heteropolymeric nature of vertebrate and bacterial ferritins, structures have been determined only for recombinant proteins constituted by a single subunit type. Herein we report the structure of *Acinetobacter baumannii* bacterioferritin, the first structural example of a heteropolymeric ferritin or ferritin-like molecule, assembled from completely overlapping Ftn homodimers harboring FOC and Bfr homodimers devoid of FOC but binding heme. The Ftn homodimers function by catalyzing the oxidation of Fe^{2+} to Fe^{3+}, while the Bfr homodimers bind a cognate ferredoxin (Bfd) which reduces the stored Fe^{3+} by transferring electrons via the heme, enabling Fe^{2+} mobilization to the cytosol for incorporation in metabolism.

Iron is an essential nutrient that functions as a cofactor of proteins participating in multiple metabolic processes. The dependency of life on iron, however, presents a dual paradox for living cells; the essential nutrient is abundant on the earth crust, but the reactivity of the Fe^{2+} ion toward O_2 makes it potentially toxic, and the insolubility of the Fe^{3+} ion renders it not readily bioavailable[1]. The challenges imposed on living cells by the chemical properties of Fe^{2+} and Fe^{3+} are ameliorated by compartmentalizing iron in ferritin and ferritin-like molecules, which are present in all three domains of life[2,3]. Ferritins, which assemble from 24 subunits into a spherical, hollow structure with octahedral (432) symmetry, catalyze the oxidation of Fe^{2+} at binuclear iron centers known as ferroxidase centers (FOC) and store the mineralized Fe^{3+} in the hollow core of the protein[4,5].

Vertebrate ferritins, which contain a variable mixture of two types of subunits, H and L, are isolated from distinct tissues with characteristic ratios of H and L subunits thought to be tuned to the ferritin function in specific tissues and organs. The genomes of many bacteria encode two types of ferritin-like molecules, the bacterial ferritins (Ftn) and the heme containing bacterioferritins (Bfr). In a few cases, such as *Neisseria gonorrhoeae* and *Magnetospirillum gryphiswaldense*, contiguous genes in a bicistronic operon code for Ftn and Bfr[6–8], suggesting that the 24-mer ferritins in these organisms are heterooligomeric, akin mammalian ferritin. In other bacteria, e.g., *Acinetobacter baumannii*, *Pseudomonas aeruginosa*, and *Escherichia coli*, the *bfr* and *ftn* genes are scattered in the genome. The recombinant expression of *ftn* or *bfr* genes from *E. coli* and *P. aeruginosa* produced homopolymeric (24-mer) proteins functional in vitro[9–11]. These observations contributed to the widespread acceptance that 24-mer homopolymers of Ftn and Bfr coexist in the bacterial cell, sharing iron storage responsibility[4,12–15]. More recently, native bacterioferritin isolated from *P. aeruginosa* cells (Pa Bfr) was found to be a heteropolymer

[1]Department of Chemistry, Louisiana State University, Baton Rouge 70803, USA. [2]Protein Structure and X-Ray Crystallography Laboratory, University of Kansas, Lawrence 66047, USA. [3]NYX, New York Structural Biology Center, Upton 10027, USA. ✉email: swlovell@ku.edu; mrivera@lsu.edu

assembled from BfrB and FtnA subunits[16]. Remarkably, the subunit content depends on the environmental O_2 concentration, ranging from almost 100% BfrB when cells are cultured in 21% O_2 to ~ 60% FtnA when cells are cultured microaerophilically.

In *P. aeruginosa*, the mobilization of iron from Pa Bfr to the cytosol requires electron transfer from bacterioferritin associated ferredoxin (Pa Bfd) to the core Fe^{3+} mineral in Pa Bfr via the Bfr-heme for subsequent mobilization of Fe^{2+}[12,17–19] (Fig. 1A). Blockade of the Bfr-Bfd complex in a *P. aeruginosa* Δ*bfd* mutant causes the irreversible accumulation of iron in Bfr, which results in intracellular iron limitation[12], metabolic dysregulation[20], and inability to mature and maintain biofilms[21]. These findings motivated the discovery of small molecule inhibitors of the Pa Bfr-Bfd complex[22], which have been shown to kill biofilm-embedded *P. aeruginosa* cells[23], thus suggesting that inhibition of iron mobilization from Bfr is a viable new target for antibiotic development[5].

Despite the well-known heteropolymeric assembly of vertebrate ferritins, and the more recently recognized heteropolymeric nature of ferritin-like molecules in pathogenic bacteria, structures have been determined only for recombinant proteins assembled from a single subunit type. Some examples are the human H, amphibian H or L ferritins[24,25], *P. aeruginosa* BfrB, and *P. aeruginosa* FtnA[9,10]. To fill this gap, we have been working on characterizing the structure of heterooligomeric bacterioferritins isolated from pathogenic bacteria. Here we report the isolation and the biochemical and structural characterization of bacterioferritin from *Acinetobacter baumannii* (Ab Bfr). This work, which produced the first structure of a heteropolymeric ferritin or ferritin-like protein, shows that the 24-mer Ab Bfr is assembled from Bfr and Ftn subunit homodimers randomly distributed on the 24-mer, such that the structure is described by an occupancy-weighted average of Bfr and Ftn subunit dimers. Moreover, only the Ftn subunits hold a viable FOC, indicating that these subunits function in the catalysis of Fe^{2+} oxidation, while the Bfr subunit dimers bind heme and form the Bfd binding site, thus enabling the mobilization of stored iron to the cytosol for incorporation in metabolism.

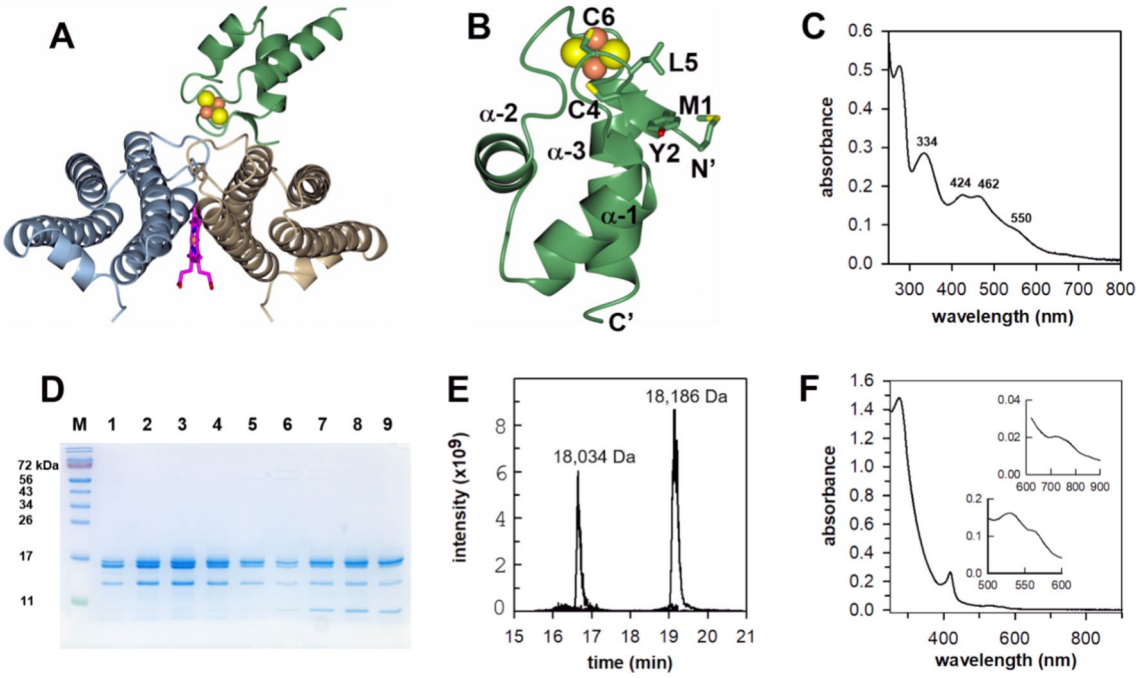

Figure 1. Isolation of Ab Bfr from *A. baumannii* cells. (**A**) Structure of the Pa Bfr-Bfd complex depicting a subunit dimer (blue and wheat) and associated heme (magenta), Bfd (green) and associated [2Fe–2S] cluster rendered as orange (Fe) and yellow (sulfur) spheres. (**B**) The Pa Bfd structure shows that a C-terminal strep tag does not interfere with the [2Fe–2S] cluster, or with the binding to Bfr, while an N-terminal tag may hinder assembly of the [2Fe–2S] because of proximity to iron ligands C4 and C6, or binding to Bfr due to proximity to residues M1, Y2, and L5, which participate at the complex interface. (**C**) UV–vis spectrum of recombinant Ab Bfd in its oxidized form. (**D**) SDS PAGE gel of fractions eluting from a Streptactin column. Cutting the bands for proteolytic digestion and LC–MS/MS analysis showed that the closely spaced bands near the 17 kDa marker have Ab Bfr and Ftn subunits, the band between the 17 kDa and 10 kDa marker contains Bfr and Ftn subunits with oxidized Met residues, and the band below the 10 kDa marker contains Ab Bfd. (**E**) The extracted ion chromatogram (EIC) obtained by LC–MS analysis of pure 24-mer Ab Bfr shows the presence of Ab Ftn subunits (18,034 kDa) and Ab Bfr subunits (18,186 kDa). The content of the Ftn (~ 39%) and Bfr (~ 61%) subunits was estimated from the corresponding peak areas in the EIC. (**F**) The UV–vis spectrum of Ab Bfr exhibits a characteristic 418 nm Soret band and a strong feature with absorption maximum ca. 300 nm, which originates from mineralized Fe^{3+} in the interior cavity. The lower inset depicts the α and β bands (567 and 530 nm), and the top inset shows the weak 740 nm band diagnostic of bis-Met coordination of the heme–iron.

Results and discussion

Purification of Ab Bfr from *A. baumannii* ATCC 17978 cells using recombinant Strep tagged Bfd

We conceived a strategy involving affinity chromatography to purify Ab Bfr, which capitalizes on the detailed understanding of the complex formed between *P. aeruginosa* Bfr and its cognate partner Pa Bfd. The structure of the *P. aeruginosa* Bfr-Bfd complex revealed that Pa Bfd binds 24-mer Pa Bfr at the interface of each subunit dimer, above each of the heme molecules, with $K_d = 4.7$ μM (Fig. 1A)[16,17,19]. Bfr and Bfd from several pathogens, including *P. aeruginosa* and *A. baumannii*, exhibit significant sequence conservation, involving residues critical to the stability of the Bfr-Bfd complex (Figure S1 and S2), suggesting that immobilized *A. baumannii* Bfd (Ab Bfd) may be used to capture Ab Bfr from cell lysates. Therefore, we synthesized the *bfd* gene from *A. baumannii* ATCC 17978 containing a C-terminal Strep-tag® and cloned it into the pET 11a expression vector (Fig. 1B). Overexpression and subsequent purification of Ab Bfd using a Streptactin® affinity column allowed the isolation of a protein with a fully assembled [2Fe–2S] cluster, as is evident in the electronic absorption spectrum (Fig. 1C), which is identical to that displayed by the well-characterized Pa Bfd[26,27].

To isolate Ab Bfr, *A. baumannii* cells were cultured aerobically in LB media supplemented with 30 μM iron. The cells were lysed, the lysate was clarified by centrifugation, mixed with a solution of Strep tagged Bfd, the resultant solution loaded onto a Streptactin® column, and the Ab Bfd-Bfr complex was eluted by passage of biotin. Analysis of the eluant fractions with the aid of SDS PAGE indicated the presence of four bands; two closely spaced bands migrate near the 17 kDa marker and are probably from bacterioferritin (Fig. 1D). The band migrating below the 11 kDa marker corresponds to Ab Bfd, and the band with electrophoretic mobility between 11 and 17 kDa is of unknown origin. These observations indicated the successful capture of Ab Bfr as a complex with Ab Bfd. To separate Ab Bfr from Ab Bfd, we capitalized on published results showing that the structure of Pa Bfd requires a phosphate ion electrostatically coordinated to the side chains of R26, R29, and K46. In the absence of phosphate, or at low ionic strength, the positively charged side chains repel and lead to loss of the [2Fe–2S] cluster and concomitant apo-protein unfolding[27]. The phosphate binding site is conserved in Ab Bfd, where the equivalent residues are R26, R29, and R46 (Figure S1). Therefore, as predicted, dialyzing the Ab Bfr-Bfd complex against 50 mM Tris (pH 7.6) facilitated the loss of the [2Fe–2S] cluster in Ab Bfd and in turn its dissociation from Ab Bfr, which enabled separation of the proteins in an anion exchange column.

Analysis of the fractions eluting from the anion exchange column containing Ab Bfr showed that the band of unknown origin was still present, so the solution was sieved through a calibrated size exclusion column with the intention of removing the unknown protein and determining the oligomerization state of the bacterioferritin. The protein eluted in a single peak with elution volume corresponding to a 24-mer. SDS PAGE analysis of the fractions showed the presence of the two closely spaced bands near the 17 kDa marker, as well as the band of unknown origin. To corroborate the identity of the proteins in the two closely spaced bands, and to determine the nature of the unknown protein, the three bands were excised from the gel and the protein in each of the bands was digested with trypsin. The ensuing peptides were analyzed by mass spectrometry, revealing that the closely spaced bands near the 17 kDa marker contain both Ftn and Bfr subunits, which indicates that 24-mer Ab Bfr molecules are assembled from Ftn and Bfr subunits. Interestingly, the SDS PAGE band of unknown origin also contained Ftn and Bfr subunits. Searching for posttranslational modifications in the peptides from this band revealed that the thioether group in several Met residues had been oxidized to sulfoxide. We speculate that the oxidized Met residues in the protein associated with this band are the reason for the unusual electrophoretic mobility.

Acinetobacter baumannii bacterioferritin is assembled from Ftn and Bfr subunits

We investigated the subunit composition of the isolated Ab Bfr with the aid of mass spectrometry. To this end, a solution of pure Ab Bfr was exchanged into ammonium acetate buffer prior to diluting in 0.1% aqueous formic acid and injecting the resultant solution into a reverse phase column for LC–MS analysis. The ion extracted chromatogram shows the presence of two peaks corresponding to the masses of Ab Ftn subunits (18,034 Da) and Ab Bfr subunits (18,186 Da) (Fig. 1E). Utilizing the integrated areas of each of the peaks in the ion extracted chromatogram to calculate the relative proportion of the subunits showed that the 24-mer Ab Bfr assembly contains ~ 39% Ftn and ~ 61% Bfr. This proportion remained consistent in four independent preparations from *A. baumannii* ATCC 17978 cultures using the methods presented in the Materials and Methods section.

X-ray Crystal structure of the heterooligomeric *Ab Bfr*

The UV–vis spectrum of the purified Ab Bfr displays a 418 nm Soret band, α- and β-bands at 567 nm and 530 nm, respectively, and a low intensity band near 740 nm (Fig. 1F). Together, these spectral bands are diagnostic of bacterioferritin where the heme–iron is axially coordinated by two Met residues[16,18,28,29]. The intense feature near 300 nm indicates that the Bfr contains an Fe^{3+} mineral core[18]. The bis-Met axial coordination of heme indicates the presence of Bfr subunit dimers in the 24-mer assembly, and by inference, the presence of Ftn subunit dimers. Whether the Bfr and Ftn subunit homodimers are randomly placed or are segregated within the 24-mer assembly cannot be discerned from the spectroscopic information. To answer this question, we crystallized Ab Bfr and determined its X-ray crystal structure.

The initial structure refinement was conducted by molecular replacement using a subunit of Pa BfrB (PDB 6NLF) as search model[23]. The initial structure solution showed eight subunits (4 subunit dimers) in the asymmetric unit, and the model revealed electron density corresponding to residues in the Bfr and Ftn sequences at each residue site in all eight subunits (Fig. 2A and B). These observations indicated that the electron density at each residue site is the average of the corresponding Ftn and Bfr subunits amino acids. Consequently, for subsequent refinement, a single subunit from Pa FtnA (PDB 3R2K)[10] was superposed to the Ab Bfr model, and the refinement was guided by both Pa BfrB (6NLF) and Pa FtnA (3R2K) structures. Modelling the Bfr and Ftn subunits required manual fitting of the residues corresponding to the Ab Bfr and Ab Ftn subunit sequences to

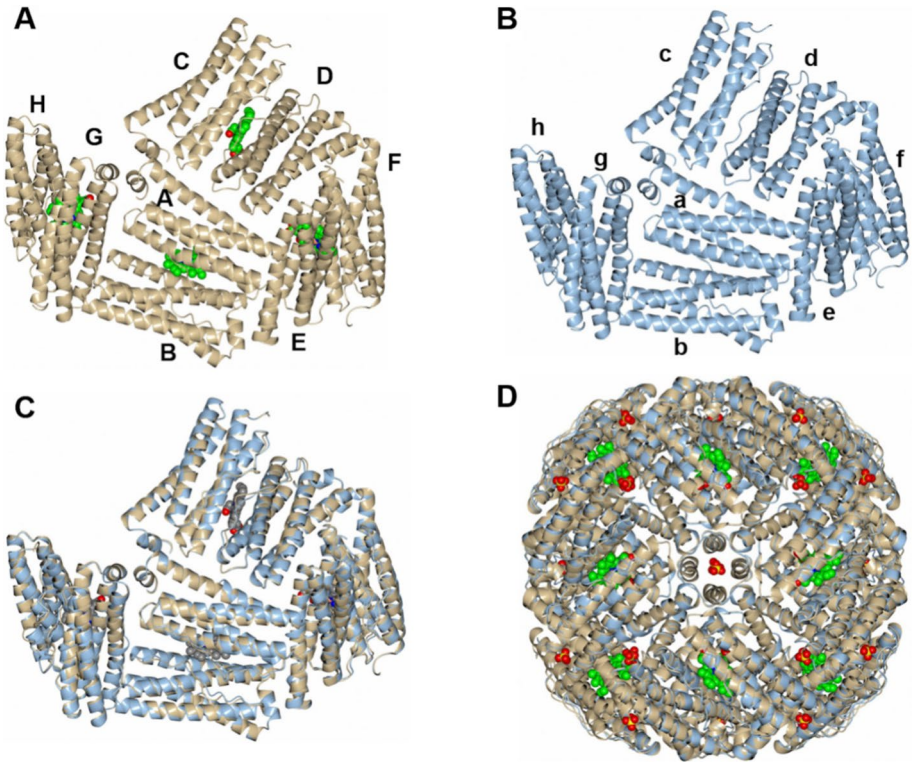

Figure 2. The X-ray crystal structure of Ab Bfr reveals a heterooligomer assembled from Bfr and Ftn subunit homodimers. (**A**) A–H indicates Bfr subunit dimers in the asymmetric unit, with each dimer binding a heme molecule (green spheres). (**B**) a–h indicates Ftn subunit dimers in the asymmetric unit. (**C**) Refined asymmetric unit composed of Bfr and Ftn subunit dimers present in a 0.56/0.44 Bfr/Ftn occupancy ratio. (**D**) 24-mer Ab Bfr biological assembly generated by crystallographic symmetry depicting the heteropolymeric structure composed of Bfr and Ftn homosubunit dimers. Sulfate ions observed in the exterior and interior cavity have been rendered as yellow/red spheres.

the electron density maps, which revealed two important observations: (i) the presence of regions where two distinct residues can be observed at the same site, and (ii) electron density from heme molecules that is associated only with the Bfr subunits (Fig. 2A). Together, these observations indicate that the structure of Ab Bfr is a heterooligomer composed of Bfr subunit dimers that bind heme, and Ftn subunit dimers. Moreover, the Bfr and Ftn subunit dimers can occupy all possible non-crystallographic symmetry related positions in the asymmetric unit, so the Ab Bfr structure is the weighted average of Bfr and Ftn subunits superimposed throughout the asymmetric unit (Fig. 2C). Therefore, structure refinement was conducted by grouping the Bfr subunits and heme molecules as group 1 (subunits A, B, C, D, E, F, G, H) and the Ftn subunits as group 2 (subunits a, b, c, d, e, f, g, h). Grouped occupancy refinement converged at occupancies 0.56 (group 1) and 0.44 (group 2), values that agree with the proportion of Bfr (61%) and Ftn (39%) subunits obtained from LC–MS analysis. Although there are only eight subunits in the asymmetric unit, the biologically relevant 24-mer assembly is readily generated by applying the crystallographic symmetry operators (Fig. 2D).

The Ab Bfr and Ab Ftn subunit sequences have 154 residues each. A sequence alignment shows approximately 37% identical, 26% similar, and 37% different residues, as well as a one-residue gap in the Ab Ftn subunit sequence at position 71, and a one-residue gap in the Ab Bfr subunit sequence at position 120 (Fig. 3A). To model the Bfr and Ftn subunits, the residues were manually fit to electron density maps, a process which revealed regions where two different residues can be observed at the same site. For example, Fig. 3B illustrates the region spanning residues 5 to 15, where position 10 shows the presence of Y10 from a Ftn subunit and Q10 from a Bfr subunit; other similar examples are shown in Figure S4. A similar correspondence of sequence number and structure can be observed for residues 1–70. The gap at position 71 in the Ab Ftn subunit sequence, however, causes an offset of the residue numbering that is realigned numerically and structurally at position 129, aided by a bulge at position 128 in the fourth α-helix of the Ftn subunit (Fig. 3C).

The electron density maps also show the presence of a heme molecule associated with each of the Ab Bfr subunit dimers, such that the heme–iron is within binding distance of the Met52 sulfur atom (Fig. 3D and E). This axial coordination of the heme–iron by two Met residues is a hallmark of the bacterioferritin structure and is consistent with the signature electronic absorption spectrum depicted in Fig. 1F. Note that the Ab Ftn subunits contain an Ala at position 52, which precludes axial coordination of the heme iron, consistent with the well-known fact that Ftn molecules do not bind heme.

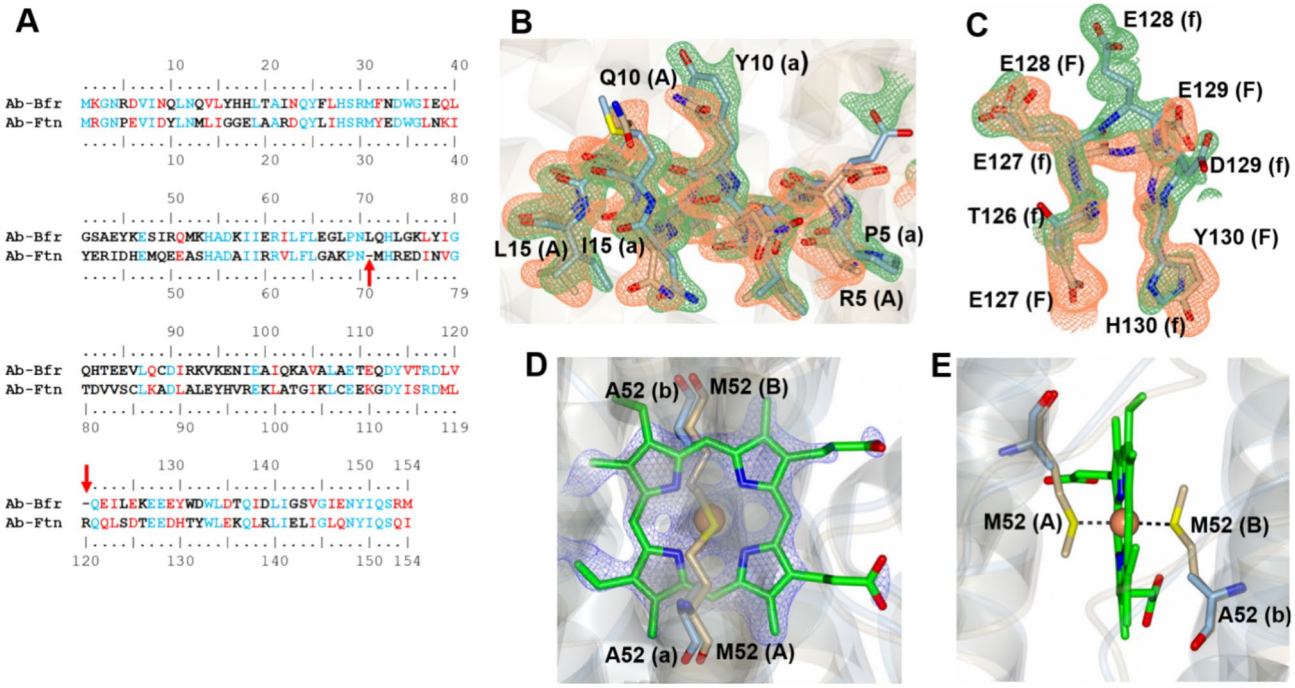

Figure 3. Amino acid sequence comparison of the Ab Bfr and Ab Ftn subunits. (**A**) Amino acid sequence alignment of Ab Bfr and Ab Ftn subunits depicting identical (cyan), similar (red) and distinct (black) residues. The arrows highlight the gaps in each of the sequences. Because the gaps are not physically present in the structures the sequence numbers corresponding to Bfr and Ftn subunits are shown above and below the corresponding sequences, respectively. (**B**) Example of modeling the mixed subunits in a portion of the Ab Bfr model. Electron density omit map contoured at (3σ) showing the residues spanning 5 to 15 in subunit A of Bfr (coral) and in subunit a of Ftn (green). Residue 10 is an example where electron density for two distinct residues can be distinguished. (**C**) Electron density omit map contoured at 3σ showing the residues spanning E127-Y130 in subunit F of Bfr (coral mesh) and T126-H130 in subunit f of Ftn (green mesh). The bulge in the helix at E128 (f) in the Ftn subunit allows the realignment of the sequence register beginning at residue 129. (**D**) 2Fo-Fc electron density map (blue mesh) for the heme molecule (green sticks) associated with the Bfr dimer composed of subunits A and B. (**E**) View illustrating the axial coordination of the heme iron (orange sphere) by the thioether atom in each of the Met52 residues in subunits A and B of a Bfr subunit dimer. Note that equivalent residue in the Ftn subunits (a and b) is Ala52, which cannot coordinate the heme iron.

The 24-mer Ab Bfr structure contains the fourfold, threefold and B-pores observed in the recombinant homopolymeric Bfr and Ftn structures. The fourfold pores in Ab Bfr are formed by four C-terminal short helices, with the side chains of Asn148 and Gln151 extending toward the pore-interior (Fig. 4A). Note that the fourfold pores formed by the Bfr and Ftn subunits are indistinguishable in sequence and structure, because the residues in the Bfr and Ftn subunits are aligned sequentially and structurally beyond residue 129. The threefold pores in Ab Bfr are formed by the proximity of three subunits, near the turn connecting helices 2 and 3. The threefold pores formed by Ab Bfr and Ab Ftn subunits are structurally identical (Fig. 4B), whereas the residues lining the B-pores of the Ab Bfr and Ab Ftn subunits are distinct (Fig. 4C). The residues lining the B-pores formed by Ab Bfr subunits are identical to those in the B-pores of recombinant *P. aeruginosa* BfrB (Figure S5A), and the residues lining the B-pores formed by Ab Ftn subunits are not fully conserved in the B-pores of Pa FtnA[9,10] (Figure S5B).

The structure of Ab Bfr is the first example of a heteropolymeric ferritin assembled from homodimeric subunits. The only other example of a heteropolymeric ferritin structure is the unique case of a secreted insect ferritin, which has an equal number of H and L subunits and is assembled exclusively from H–L heterodimers, with FOC present only in the H subunits. The exclusive presence of heterodimers eliminates the twofold axes of symmetry and lowers the octahedral (432) symmetry characteristic of ferritins to tetrahedral, enabling a symmetrical, rather than a random arrangement of heterosubunits[30]. Moreover, the complete overlap of two subunits across the structure is not encountered often. In fact, a search of the ~ 215,000 entries in the Protein Databank (excluding those determined by NMR and cryo EM) for structures that contain an entire subunit where all residues have been refined with partial occupancy revealed only one other similar case, the complex of pseudoenzymes PDX1.2 and its cognate enzyme PDX1.3 from *Arabidopsis thaliana* which form dodecameric structures[31]. The structural similarity between these two proteins resulted in crystals in which the PDX1.2 and PDX1.3 proteins overlapped in the asymmetric unit and were each modeled with 0.5 occupancy.

Only the Ftn subunits in Ab Bfr harbor a FOC

Sequence alignments of Bfr from pathogens representative of the enterobacteriales (*E. coli*, *E. cloacae*, *K. pneumoniae*), pseudomonadales (*P. aeruginosa*) and moraxellales (*A. baumannii*) groups show conservation of the

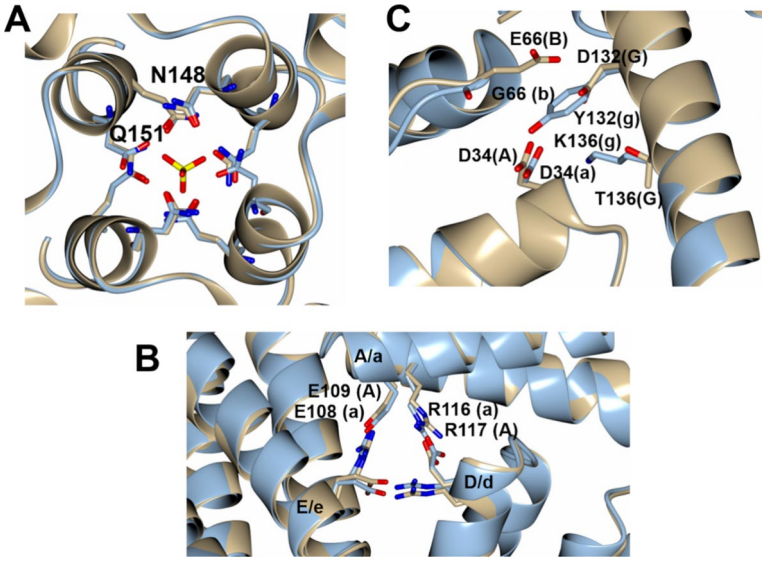

Figure 4. The pores in Ab Bfr which communicate the protein exterior with the interior. (**A**) Closeup of a four-fold pore viewed along a four-fold axis depicting the side chains of N148 and Q151 pointing toward the pore interior. The fourfold pores formed by Ab Ftn subunits (light blue) and Ab Bfr subunits (tan) are identical in sequence and structure. A sulfate ion can be observed in the protein interior, near the fourfold pore but not in contact with Q151. (**B**) A three-fold pore formed by the Ftn (light blue) and Bfr (tan) subunits. The interior of the threefold pore formed by Bfr subunits is lined by the side chains of E109 (A) and R117 (A), whereas the pore formed by Ftn subunits is lined by the side chains of E108 (a) and R116 (a). Note that although the sequence is offset by one residue, the pore structures are identical. (**C**) A B-pore formed by the Ab Bfr subunits (tan) is lined by the side chains of D34 (A), E66 (B), D132 (G) and T136 (G), while the equivalent B-pore formed by Ab Ftn subunits is lined by D34 (a), G66 (b), Y132 (g) and K136 (g).

FOC ligands, with the binuclear iron center coordinated by E18, E51, H54, E94 and H130. However, only one of these residues (H54) is conserved in moraxellales (Figure S2). These observations suggest that the FOC in Ab Bfr subunits exhibits a previously uncharacterized set of ligands, or that Ab Bfr does not contain FOC. A similar alignment of Ftn sequences (Figure S3) reveals that the Ab Ftn subunits and Pa Ftn share the same set of FOC ligands (E18, E51, H54, E93, and H130), which differ from those in the Ftns from *E. coli* and *E. cloacae*, which have a glutamate at position 130.

The structure of Ab Bfr did not show iron, or any other metal ion coordinated at FOC. Several attempts at soaking the crystals in Fe^{2+} solution to populate the FOC with iron, as we have done successfully for recombinant bacterioferritin structures[9,10,32], resulted in the dissolution of the crystals, or in poor diffraction. Hence, to begin understanding the nature of the FOC in Ab Bfr, we superposed Ab Ftn (subunit a) with the structure of recombinant Pa FtnA binding iron at the FOC (PDB 3R2L)[10], which resulted in Cα RMSD = 0.50 Å (153 residues). Focusing on the FOC (Fig. 5A) reveals that as predicted from the sequence alignment, the FOC in the Ab Ftn subunits are probably identical to those in the structure of Pa FtnA, where E18 and H54 are terminal ligands to Fe1, E51 coordinates to Fe1 and Fe2, and E93 and H130 are terminal ligands coordinating to Fe2; the conformation of the H130 side chain in the Ab Ftn subunits is rotated away from Fe2, in a pose nearly identical to the gate-open conformation observed in the structure of recombinant Pa FtnA (3R2H) and Pa BfrB not bound to iron (PDB 3ISF)[9,10]. The proposed structure of a binuclear FOC in the Ab Ftn subunits (Fig. 5A) is also predicted by a model generated using AlphaFold 3[33] (Fig. 5B).

A similar structural superposition of the Ab Bfr subunit A with the structure of recombinant Pa BfrB binding iron at the FOC (PDB 3IS8)[9] resulted in Cα RMSD of 0.51 Å (153 residues) (Fig. 5C). The alignment suggests that a putative binuclear iron center in Ab Bfr subunit may be coordinated by H18 and H54 as ligands to Fe1, and E127 and Q51 as ligands bridging Fe1 and Fe2. The side chains of E47 and N97 are in proximity to the iron and in principle could function as ligands to Fe2. When AlphaFold 3 was used to predict the structures of the FOC in Ab Bfr, however, the predicted structure indicates that only one iron is present, coordinated by H18, H54, Q51, and E127 (Fig. 5D). Taken together, these observations suggest that the Ab Bfr subunits probably do not harbor a FOC.

To further test this idea, a recombinant gene coding for Ab bacterioferritin was overexpressed, and the recombinant 24-mer protein was purified. The UV–vis spectrum of recombinant Ab bacterioferritin (Figure S6) shows the characteristic features of bis-Met coordinated heme, the absorbance near 320 nm indicates the absence of an Fe^{3+} core, and the analysis of heme content revealed the presence of one heme molecule/24-mer. To assess whether the FOC in the recombinant Ab bacterioferritin are active, the protein was titrated with Fe^{2+} to a total of 500 Fe^{2+}/24-mer and the mixture was passed through a size exclusion column from which two peaks eluted (Figure S7A). The first peak contained 24-mer protein but no iron, while the second peak was devoid of protein but contained iron, and the UV–vis spectrum of the protein in the first peak is identical to the spectrum obtained

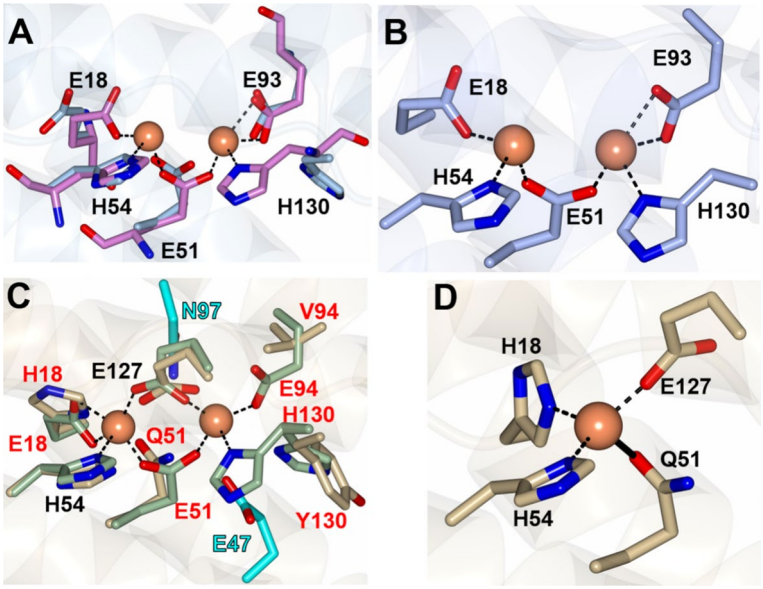

Figure 5. The ferroxidase centers in Ab Bfr. (**A**) Superposition of an Ab Ftn subunit (blue) and a Pa Ftn subunit (lilac) bound to iron (orange spheres, PDB 3R2L) indicates that E18, H54, E51, E93 and H130 in Ab Ftn function as ligands to a binuclear iron ferroxidase center. The conformation of H130 in Pa Ftn has been shown to change from the gate open in the apo-form (PDB 3R2H), which is like the H130 conformation exhibited by the Ab Ftn H130 side chain, to the gate closed in the iron bound form. (**B**) The FOC structure of Ab Ftn subunits predicted by AlphaFold 3 is identical to that in the structural superposition in panel A. (**C**) Superposition of an Ab Bfr subunit (tan) and a Pa Bfr subunit (olive) bound to iron (PDB 3IS8); the side chain of H130 in the Pa Bfr structure is in the gate closed (coordinated) and gate open conformations. In the superposed structures, the relative proximity of residues H18, H54, Q51, E47, and E127 in the Ab Bfr subunit to the iron ions suggest that these residues may coordinate iron in Ab Bfr. Note that conserved residues are annotated in black font and residues that are different are annotated in red. Residues N97 and E47 (cyan) are included because of their relative proximity to the iron ions. (**D**) The FOC structure of Ab Bfr subunits predicted by AlphaFold 3 binds a single iron, and therefore supports the idea that the Ab Bfr subunits do not bind binuclear FOC sites (the longer contact made Q51 (2.64 Å) is indicated by a solid line). This conclusion is mirrored in the absence of ferroxidase activity exhibited by a recombinant 24-mer assembled only from Pa Bfr subunits (see text).

prior to the titration (Figure S7B). These observations indicate that recombinant Ab Bfr, and by extension the Bfr subunits in Ab Bfr, do not contain a competent FOC and therefore cannot catalyze the oxidation of Fe^{2+}. In comparison, a similar experiment with recombinant 24-mer Pa BfrB, which harbors a competent FOC in each subunit[9], shows that the protein eluting in the first peak (Figure S7C) contains ~ 280 Fe /24-mer, which is evident in the increased absorbance ca. 320 relative to that in the spectrum prior to the titration (Figure S7D). Therefore, it can be concluded that Ab Bfr is assembled of Ftn subunits containing a FOC and Bfr subunits lacking a FOC, a situation reminiscent of vertebrate ferritins assembled from H and subunits.

The Bfd binding site on Ab Bfr is structurally conserved

The mobilization of Fe^{3+} from Pa Bfr to the cytosol of *P. aeruginosa* requires the binding of Pa Bfd[12,20]. Pa Bfd binds Pa Bfr at sites located at the interface of each Bfr homodimer, enabling electron transfer from the [2Fe–2S] cluster in Pa Bfd to the Fe^{3+} mineral in the interior cavity via the heme in Pa Bfr, thus promoting Fe^{2+} mobilization (Fig. 1A)[4,17,19]. The Pa Bfd binding site on the Pa Bfr surface is a shallow depression delineated by residues L68, P69, N70, and Q72 from one subunit (blue), and L78, L79, G80 and E81 from the accompanying subunit (wheat), where Pa Bfd residues M1, Y2, and L5 can bind (Fig. 6A and B)[5,17]. The residues at the Pa Bfr-Pa Bfd complex interface are conserved in Ab Bfr and Ab Bfd (Figures S1 and S2), therefore suggesting structural conservation of the Bfr-Bfd interface. To test this idea, we superposed the Ab Bfr structure onto the structure of the Pa BfrB-Bfd complex and then modeled an AlphaFold-predicted structure of Ab Bfd merged with the [2Fe–2S] cluster of the Pa Bfd structure. The results (Fig. 6C and D) show that the Bfd-binding site on Ab Bfr is similar to that on Pa Bfr, where the conserved M1, Y2 and L5 residues of Ab Bfd are expected to bind in a manner similar to that observed in Pa Bfd-Pa BfrB complex.

We used surface plasmon resonance (SPR) to measure the strength of the interaction between Ab Bfr and Ab Bfd. Flowing Ab Bfd over Ab Bfr immobilized on a sensor chip produced the responses shown in Fig. 7A. The plateau reached in each of the responses indicates steady state equilibrium, so plotting each response at steady state as a function of the Bfd concentration results in the hyperbolic binding curve described by the black circles in Fig. 7B. Fitting the curve shows that Ab Bfd binds to Ab Bfr with $K_d = 5.6$ μM, a value similar to that

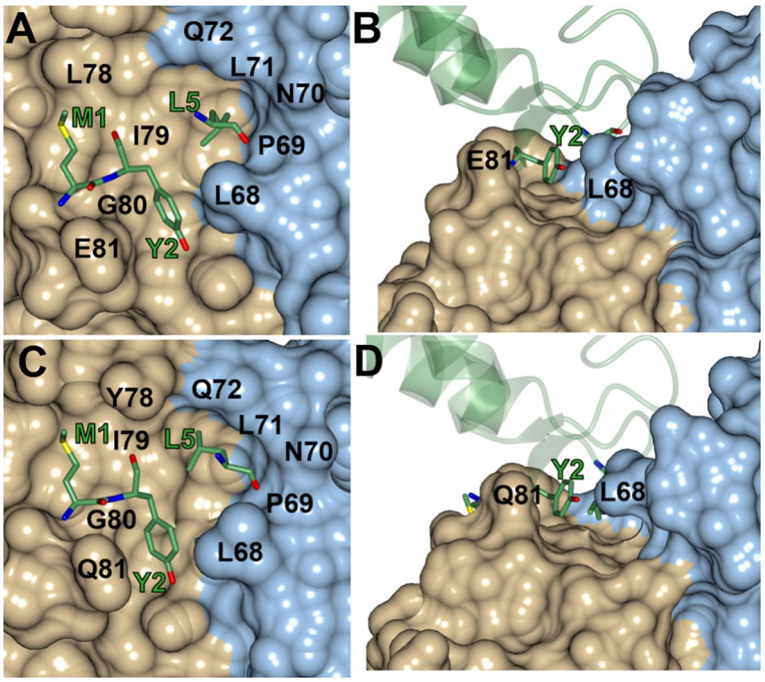

Figure 6. Comparison of the Bfd-binding site in Pa Bfr and Ab Bfr. (**A**) Closeup view of the Bfd-binding site on Pa Bfr homodimer where residues L68, L71, and Q72 in one subunit (blue), and L78, I79 G80 and E81 in the accompanying subunit (wheat) form a shallow depression where residues M1, Y2 and L5 (green sticks) from Pa Bfd anchor. (**B**) Same as panel A but rotated approximately 90 degrees in the horizontal direction to illustrate the shallow cleft formed by the side chains of L68 and E81 in Pa Bfr. (**C**) Closeup view of the Bfd-binding site on an Ab Bfr subunit dimer (wheat and blue surface rendering) where an AlphaFold model of Ab Bfd has been modeled. The structure of the Bfd-binding site in Ab Bfr is similar to that of Pa Bfr, where residues M1, Y2 and L5 from Ab Bfd are expected to bind. (**D**) Same as panel C but rotated approximately 90 degrees in the horizontal direction to show the shallow cleft formed by L68 and Q81.

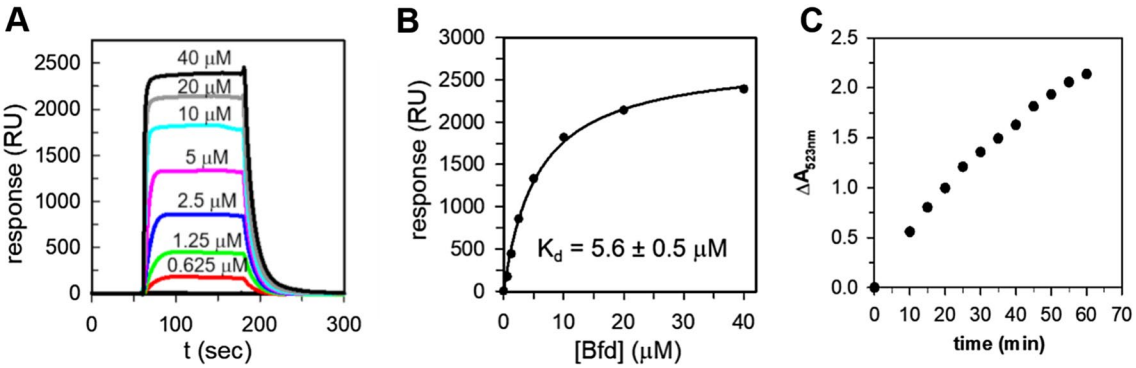

Figure 7. Ab Bfd binds Ab Bfr in solution. (**A**) The association between Ab Bfr and Ab Bfd was studied with the aid of SPR. Reference and baseline subtracted responses measured on flowing Ab Bfd solution of concentrations indicated in the figure over immobilized Ab Bfr. (**B**) The binding affinity was determined by steady state analysis. The steady state responses shown in panel A were plotted as a function of Bfd concentration (black circles) and fitted to the binding mode (solid line) described by Eq. 2. (**C**) Time-dependent release of Fe^{2+} from Ab Bfr assessed by the increase of normalized ΔA_{523} upon addition of excess NADPH to a solution containing Ab Bfr, Ab Bfd, Pa Fpr, and bipyridine.

measured for the binding of Pa Bfd to Pa Bfr (4.7 μM)[16]. These findings, which agree with the conservation of the Bfd binding site on Ab Bfr, indicate that iron mobilization from Ab Bfr requires binding and electron transfer from Ab Bfd. To further assess this idea, we resorted to an assay previously developed with the proteins from *P. aeruginosa*, where NADPH is added to a solution containing Bfr, Bfd, Fpr (ferredoxin NADP reductase), and the Fe^{2+} chelator bipyridine. Electrons from NADPH are transferred to the flavin in Fpr, which reduces the [2Fe–2S] cluster of Bfd, which in turn transfers electrons to the Fe^{3+} mineral in Bfr via the heme (see Fig. 1A). The resultant

Fe^{2+} exit the bacterioferritin and are coordinated by bipyridine, resulting in a peak with maximum absorbance at 523 nm[17,18]. The results from this assay conducted by the addition of NADPH to a solution containing Ab Bfr, Ab Bfd, Pa Fpr, and bipyridine (Fig. 7C) show the mobilization of iron from Ab Bfr, thus supporting the idea that Ab Bfd binds Ab Bfr and transfers electrons to the ferric mineral core in the bacterioferritin.

Why is Ab Bfr assembled entirely from Bfr and Ftn homodimers?

The structure of Ab Bfr is the first example of a heteropolymeric ferritin or ferritin-like molecule. In this context, it is noteworthy that despite the well-recognized heteropolymeric nature of vertebrate ferritins, which are assemblies of H and L subunits[34], structures have been determined only for recombinant proteins assembled from a single subunit type, such as human H, or amphibian H or L[24,25], and for native ferritins modeled with a single predominant subunit[35]. In contrast to the case of vertebrate ferritins, until recently, it was thought that 24-mer homopolymers of Ftn and Bfr coexist in the bacterial cell. This belief changed with the demonstration that *P. aeruginosa* utilizes a heteropolymeric bacterioferritin assembled from FtnA and BfrB subunits[16]. Although this study suggested that the heteropolymeric Pa Bfr is probably an assembly of BfrB and FtnA subunit homodimers, the distribution of homodimers in the 24-mer was unknown. The crystal structure of Ab Bfr reported here firmly establishes that the heteropolymeric 24-mer is an assembly of Ftn and Bfr subunit homodimers and shows that their distribution in the 24-mer architecture is random.

These findings lead to question why do heterooligomeric bacterioferritins assemble exclusively from Bfr and Ftn homodimers? The answer is certainly related to two main issues: (*i*) Satisfying the unique microenvironment of the heme bound to Bfr homodimers: The C2 axis of symmetry in a Bfr homodimer passes through the heme iron, which can be axially coordinated only by the Met52 side chain from each of the subunits (Fig. 3E). Since the axial bis-Met coordination of the heme–iron is important to tune the electronic and redox properties of the bacterioferritin heme, this specialized microenvironment cannot be satisfied in Bfr-Ftn heterodimers because Ftn subunits do not have a Met at position 52. (*ii*) Creating the Bfd binding site at the protein surface, which is formed at the interface of Bfr subunit homodimers. Bfr-Ftn subunit heterodimers are not suited to replicate the surface microenvironment that allows Bfd to bind and enable core iron mobilization, a process that involves electron transfer from the [2Fe–2S] cluster in Bfd to the ferric mineral in the 24-mer interior cavity via the heme in Bfr subunit homodimers (see Fig. 1A).

Given the significant role played by Bfr subunit homodimers in binding heme and Bfd, it is important to consider how Bfr and Ftn homodimers are selected. There is no conservation of dimer interface residues between Ftn and Bfr, and comparing the dimer interface of an Ab Bfr and Ab Ftn subunit homodimers with that of a putative Ab Bfr-Ftn subunit heterodimer is illustrative. The homodimeric Bfr subunit interface exhibits stabilizing H-bonding and electrostatic interactions across the entire interface (Fig. 8A–C), and a similar situation can be observed at the homodimer Ftn subunit interface (Figure S8). In contrast, the putative Bfr-Ftn subunit heterodimer model shows only a few H-bonds across the interface and repulsive electrostatic interactions (Fig. 8D–F).

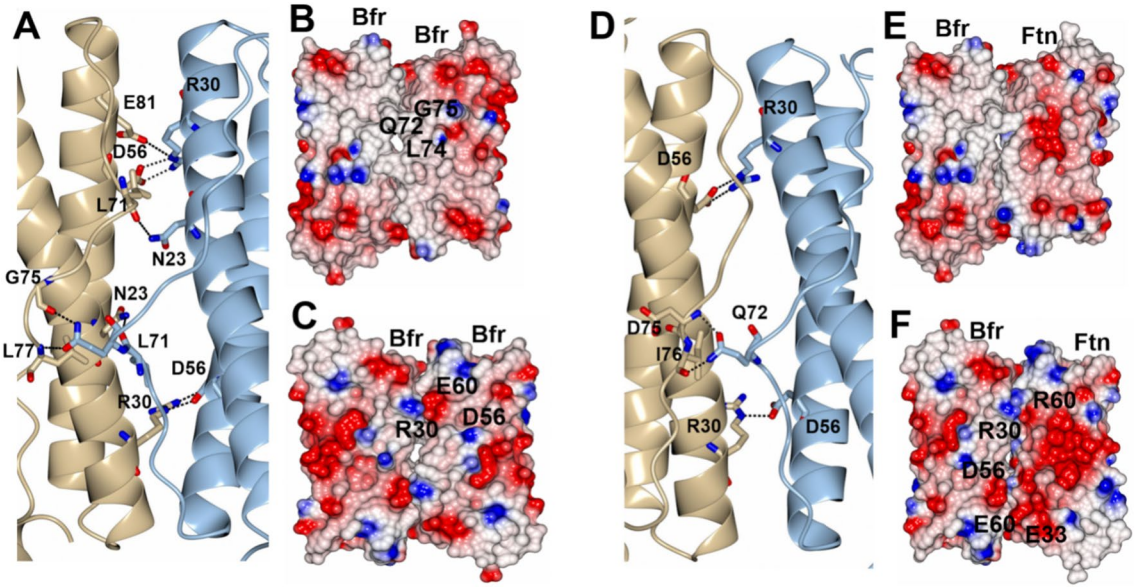

Figure 8. Favorable electrostatic and H-bonding interactions select for Bfr and Ftn homodimers. (**A**) Ribbon view of an Ab Bfr subunit dimer (heme not shown) highlighting hydrogen bonding (dashed lines) interactions stabilizing the dimer. (**B**) Electrostatic surface representation (−0.5 V (red) to 0.5 V (blue)) of an Ab Bfr homodimer viewed from the protein exterior, and (**C**) from the protein interior. (**D**) Ribbon view of a theoretical Ab Bfr-Ftn heterodimer where the Bfr subunit is depicted in blue and the Ftn subunit in wheat, with H-bonds indicated by dashed lines. (**E** and **F**) Electrostatic surface representation of the putative Ab Bfr-Ftn heterodimer viewed, respectively, from the protein exterior and interior.

Together, these observations support the idea that homodimers are selected to ensure proper heme binding, as well as formation of Bfd binding sites, both of which function in the mobilization of iron from the core.

In conclusion, the structure of Ab Bfr is the first example of a heteropolymeric ferritin or ferritin-like molecule assembled from homodimers of Ftn and Bfr subunits. The Ftn subunit dimers have FOC and therefore function in the oxidation of Fe^{2+}, while the Bfr subunit dimers which bind heme, function in iron mobilization by binding Bfd and therefore enabling reduction the Fe^{3+} mineral to facilitate the release of Fe^{2+} to the cytosol for its incorporation in metabolism.

Methods

Recombinant Ab Bfr and Ab Bfd expression systems

The genes coding *A. baumannii* ATCC 17978 Bfr and Bfd (see Data Accessibility), engineered to introduce codons favored by *E. coli*, were synthesized and each cloned into the pET-11a vector (Gene Script, Piscataway, NJ) using Nde I and BamHI restriction sites (Figures S9 and S10). The *bfd* gene was synthesized with a Strep-tag (WSHPQFEK) fused at the C-terminal end. The pET-11a-*bfr* was transformed into *E. coli* BL21-Gold (DE3) cells (Agilent Technologies) and the pET-11-a-*bfd* construct was transformed into *E. coli* Arctic Express RIL cells (Agilent Technologies).

Expression and purification of Strep-tagged Ab Bfd

Pre-cultures of *E. coli* Arctic Express RIL cells transformed with pET-11-a-*bfd* were grown in Terrific Broth (TB) (50 mL, 14 h, 37 °C, 220 rpm) in the presence of 100 µg/mL ampicillin and 20 µg/mL gentamycin and used to inoculate 1 L TB with no antibiotics. The 1-L cultures were grown in TB for ~ 2.5 h (37 °C, 220 rpm) before transferring to a 10 °C-equilibrated incubator and shaken (220 rpm) for 45 min. The cultures were then induced by addition of 1 mM isopropyl-D-1-thiogalactopyranoside (IPTG), and then cultured 24 h before cell harvesting by centrifugation (4 °C, 4392 × *g*, 20 min) and storage at -80 °C. Cells were resuspended in 75 mL lysis buffer (50 mM potassium phosphate (pH 7.6), 5 mM dithiothreitol (DTT), 1 mM phenylmethyl sulfonyl fluoride (PMSF), 4.2 mM $MgSO_4$, 50 mg lysozyme, 5 mg DNase, 50 mg deoxycholic acid, 1 tablet of protease inhibitor cocktail (Pierce), 1% Triton X-100), stirred at room temperature (20 min) and then lysed on ice with a Qsonica Q500 sonicator (60% pulse amplitude, 15 cycles, 10 s pulse on, 50 s pulse off). The lysate was clarified by centrifugation (4 °C, 52,755 × *g*, 30 min), diluted twofold with buffer 1 (50 mM potassium phosphate (pH 7.6), 5 mM DTT), loaded onto a Q-sepharose column equilibrated with buffer 1 and eluted with buffer 1 containing 600 mM NaCl. The fractions containing Ab Bfd were pooled, diluted twofold with buffer 2 (50 mM potassium phosphate, 150 mM NaCl, 5 mM DTT, pH 7.6), loaded onto a StrepTrap™ XT 5 mL column (Cytiva) using an AKTA Pure FPLC, and eluted with buffer 2 containing 50 mM biotin. Fractions containing Ab Bfd were concentrated, passed through a PD-10 desalting column (Cytiva) to remove the biotin, and then stored at -80 °C.

Isolation of Ab Bfr from *A. baumannii* ATCC 17978 cells

A. baumannii cells were cultured (2L, 37 °C, 220 rpm, 24 h) in LB media supplemented with 30 µM ferrous ammonium sulfate, $(NH_4)_2Fe(SO_4)_2$, harvested by centrifugation (4 °C, 4392 × *g*, 20 min), and stored at -80 °C. The cells were resuspended in lysis buffer (see above), stirred at room temperature for 15 min, then lysed on ice using a Qsonica Q500 sonicator (65% pulse amplitude, 10 s on, 50 s off, 20 cycles). The lysate was clarified by centrifugation (4 °C, 52,755 × *g*, 60 min), and the supernatant was dialyzed (4 °C) against 50 mM potassium phosphate buffer pH 7.4 and filtered through a 0.22 µm filter. Strep tagged Bfd (1 mg) was added to the cell extract, the solution was incubated on ice for 45 min, and then loaded onto a StrepTrap™ XT 5 mL column using an AKTA Pure FPLC. The column was washed with buffer H (50 mM potassium phosphate, 150 mM NaCl, 5 mM DTT, pH 7.6) and eluted with buffer H containing 50 mM biotin. The fractions containing Ab Bfr were pooled and the buffer was exchanged to buffer D (50 mM Tris, pH 7.6, 1 mM TCEP, 1 tablet protease inhibitor cocktail) using an Amicon Ultra Centrifugal filter (50 kDa MWCO). The resultant solution was loaded onto a Source™ 15Q column (Cytiva) equilibrated with buffer D and eluted with buffer D and an NaCl gradient (0 to 600 mM NaCl). The oligomerization state (24-mer) of the isolated Ab Bfr was confirmed by passage of the pure protein through a calibrated Superdex™200 Increase GL size exclusion column equilibrated and eluted 100 mM potassium phosphate, 1 mM TCEP, pH 7.5.

Expression and purification of recombinant Ab Bfr

Pre-cultures of *E. coli* BL21-Gold (DE3) cells transformed with the pET-11a-*bfr* construct grown (14 h, 37 °C, 220 rpm) in 50 mL TB containing 50 µg/mL ampicillin were used to inoculate 1 L cultures of TB (30 °C, 220 rpm, no antibiotic). Protein expression was induced with 0.25 mM IPTG when the OD_{600nm} reached 0.6. The cells were harvested by centrifugation (4 °C, 4392 × *g*, 20 min) 3 h later and stored at -80 °C. The cells were resuspended (3 mL/g of cells) in lysis buffer (50 mM Tris-base pH 8.0, 5 mM DTT, 5 mM potassium phosphate, 100 mM NaCl, 0.5 mM PMSF, 1% Triton X-100, 2 mg/mL lysozyme, 1.6 mg/mL deoxycholic acid, 0.1 mg/mL DNAse, 4.2 mM $MgSO_4$, and a tablet of Pierce™ protease inhibitor), stirred (30 min) at room temperature and then incubated (5 min) at 30 °C. The cells were sonicated (70% pulse amplitude, 12 cycles, 15 s pulse on, 45 s pulse off), and the lysate was centrifuged (4 °C, 52,755 × *g*, 50 min). The supernatant was dialyzed against buffer A (50 mM Tris, 5 mM potassium phosphate, 1 mM TCEP, pH 8.5), filtered (4.5 µm nylon filter, VWR), and loaded onto a column (26 mm in diameter) packed with ~ 30 mL of Q Sepharose Fast Flow anion exchange resin (Sigma-Aldrich, St. Louis, MO, USA) equilibrated with buffer A and eluted with a KCl gradient (0 to 650 mM). Fractions containing Ab Bfr were dialyzed against buffer A and chromatographed a second time on a Q Sepharose anion exchange column. The Ab Bfr was dialyzed against buffer B (50 mM Tris-base, 5 mM potassium phosphate, 1 mM TCEP, pH 8.0), loaded onto a 10 mL hydroxyapatite column (Bio-Scale™ Mini CHT™ Type 1, 40 µm cartridge,

BIO-RAD), and eluted with a 5 to 800 mM potassium phosphate gradient (pH 8.0). Ab Bfr 24-mer was separated from incompletely assembled protein in a Superdex™200 Increase 10/300 GL size exclusion column equilibrated and eluted with buffer B. The 24-mer Ab Bfr was dialyzed against buffer A, chromatographed on a Source™ 15Q column equilibrated with buffer A and eluted with a 65 to 585 mM KCl gradient. Pure 24-mer bacterioferritin was confirmed by passage through a calibrated Superdex™200 Increase 10/300 GL size exclusion column equilibrated and eluted with buffer B. The protein concentration was determined by the Bradford assay (Bio-Rad Protein Assay Kit), and pure protein was flash-frozen and stored at − 80 °C.

Crystallization and data collection

To screen for crystallization conditions, purified *Ab*-Bfr was concentrated to 12.5 mg/mL in 100 mM sodium potassium phosphate (pH 7.5), 1 mM TCEP. All crystallization experiments were set up using an NT8 drop setting robot (Formulatrix Inc.) and UVXPO MRC (Molecular Dimensions) sitting drop vapor diffusion plates at 18 °C. 100 nL of protein and 100 nL crystallization solution were dispensed and equilibrated against 50 uL of the latter. Prismatic, red crystals were observed overnight from the Berkeley Screen[36] (Rigaku Reagents) condition E5 (1.2 M ammonium sulfate, 100 mM bis–tris pH 6.5). Samples were transferred to a cryoprotectant solution composed of 80% (w/v) crystallant and 20% (v/v) glycerol before storing in liquid nitrogen. X-ray diffraction data were collected at the National Synchrotron Light Source II beamline 19-ID (NYX) using an Eiger2 X 9 M pixel array detector.

Structure solution and refinement

Intensities were integrated using XDS[37,38] and the Laue class analysis and data scaling were conducted with Aimless[39]. Structure solution was conducted by molecular replacement with Phaser[40] using a single subunit of a previously determined Pa Bfr structure (PDB 6NLF[22]) as the search model. The top solution was obtained in the space group *P*23 and contained eight molecules in the asymmetric unit. Following initial refinement, electron density for the Ftn protein was observed at each residue site and in all eight subunits. Effectively, all subunits contained the average content of both Bfr and Ftn polypeptides at the same sites. Therefore, a single subunit from a previously determined Pa Ftn subunit (PDB 3R2K[10]) was superimposed onto the Bfr subunits and the 6NLF and 3R2K structures was used as reference models in the early stages of refinement with Phenix[41]. Electron density consistent with heme molecules associated with the Bfr subunits was observed. Manual model building and refinement were performed with Coot[42] and Phenix, respectively. Group occupancy refinement was carried out with the following groups: Group 1: Ab Bfr subunits A, B, C, D, E, F, G, H and the heme molecules, Group 2: Ab Ftn a, b, c, d, e, f, g, h. The occupancies refined to 0.56 for group 1 and 0.44 for group 2. Reference model restraints were not used in the later stages of refinement and non-crystallographic symmetry restraints were applied. Structure validation was conducted with Molprobity[43] and figures were prepared using the CCP4MG package[44]. Structure superposition was conducted with GESAMT[45]. Crystallographic data are provided in Table S1.

Mass spectrometric determination of Bfr and Ftn subunit content in purified Ab Bfr

Ab Bfr solution (500 µL) was buffer exchanged into 10 mM NH_4HCO_3 pH 7.8, 1 mM TCEP using Amicon Ultra filtration units (3 cycles). The solution was diluted in aqueous 0.1% formic acid to ~ 1 µM protein concentration and then incubated (15 min) at 25 °C. Bfr and Ftn content analysis was conducted with a Dionex Ultimate 3000 LC (Thermo Scientific, Walthman, MA, USA) coupled to a Bruker Amazon Speed ETD Ion Trap mass spectrometer (Bruker, Billerica, MA, USA). Samples (5 µL) were separated (60 °C, 0.4 mL/min) in a Poroshell 120 EC-C8 column (2.0 × 100 mm, 2.7 µm particle size, 120 Å pore size; Agilent, Santa Clara, CA, USA). The mobile phase (MP) composition was A: 0.1% aqueous formic acid; B: 0.1% formic acid in acetonitrile. Initial = 5% B (2 min), increase to 50% B over 19 min, increase to 90% B over 2 min, hold at 90% B for 4 min, return to initial in 1 min, and equilibrate (6 min). The ion trap was in positive UltraScan mode with electrospray voltage = 4500 V and endplate voltage = 500 V. The nebulizer operated at 35 psi (N_2, 10 L/min) and drying T = 250 °C. Spectra was acquired with maximum accumulation time of 50 ms and ion charge control = 250,000. Proteins were detected in full scan mode (400–2000 m/*z*), averaging five spectra in both profile and centroid mode. LC–MS data was processed using Bruker Compass Data Analysis 4.0 utilizing the mass spectra deconvolution tool to automate the calculation of molecular masses of components in the mixture. Charge deconvolution was conducted over a range of 5–30 kDa with a 10% abundance cutoff. Extracted ion chromatograms were generated for the subunits of Bfr (18,186 Da) and Ftn (18,034 Da) using the m/*z* values from the three most abundant charge states in the deconvolution, followed by application of a 23-point Savitzky–Golay filter to smooth the reconstructed spectra. The peaks were integrated, and the relative percentage of Ftn in the sample was calculated using Eq. (1).

$$\%Ftn = \frac{(Ftn\ peak\ area)}{(Ftn\ peak\ area + Bfr\ peak\ area)} \quad (1)$$

In-gel digestion and mass spectrometric characterization of proteins

SDS-PAGE bands were cut, and the proteins were subjected to proteolytic digestion as previously described[16]. Dried extracts were dissolved in 50 µL 0.1% formic acid for LC–MS analysis in a Dionex Ultimate 3000 RSLC system coupled to a Q-Exactive Orbitrap spectrometer (Thermo Scientific, Walthman, MA, USA). Samples (1 µg) were loaded onto a trap column (C18 PepMap 100, 5 µm, and 100 Å) at 20 µL/min using 2% B (see above for mobile phase composition). Peptides were then separated in an analytical column (Acclaim PepMap 100 (C18), 3 µm, 100 Å) at 0.3 µL/min as follows: hold at 5% B (7 min), increase to 10% B (1 min), increase to 25% B (14 min), increase to 90% B (1 min), hold at 90% B (5 min), return to 5% B (1 min), and equilibrate (4 min).

Nano electrospray ionization was performed with a stainless-steel emitter (50 µm ID) held at 2.0 kV. Spectra were acquired in data dependent mode with a loop count of 10. Full scans and MS2 scans were acquired with resolutions of 70,000 and 17,500, respectively, isolating ions in a 1.6 m/*z* window with normalized collision energy = 28. Raw files were analyzed using Proteome Discoverer (version 2.4, Thermo Scientific) searching with SEQUEST HT (Thermo Scientific, Walthman, MA, USA) and Mascot (Matrix Science, London, UK). Data files were searched against the transcriptomics derived database[46].

Recombinant bacterioferritin Fe^{2+} oxidation and mineralization

A 10 mM solution of ferrous ammonium sulfate ($NH_4Fe(SO_4)_2$) was prepared by dissolving the ferrous salt in water containing 5µL/10 mL of concentrated HCl. 24-Mer Ab Bfr (0.65 mL, 1.0 µM) in 50 mM Tris, 5 mM potassium phosphate, 1 mM TCEP, pH 8.0 was placed in a 1.0 cm cuvette containing a magnetic bar and titrated with the $NH_4Fe(SO_4)_2$ solution under continuous stirring. Each aliquot delivered 100 Fe^{2+}/24-mer to a total of 500 Fe^{2+}/24-mer, allowing 10 min in between aliquots. The process was monitored spectrophotometrically with a Cary 50 spectrophotometer. The resultant solution was incubated overnight at 4 °C and then passed through a calibrated Superdex™ 200 Increase 10/300 GL size exclusion column. The iron content in the protein core was determined as follows[47]: 50 µL of concentrated HCl was added to 50 µL of mineralized Ab Bfr and the mixture was incubated for 15 min before the addition of 50 µL ascorbic acid (25 mg/mL) and 250 µL of saturated aqueous sodium acetate. After 15 min incubation, 50 µL of ferrozine (5 mg/mL) was added and the solution was incubated for 15 min. The iron concentration was determined using the absorbance at 562 nm ($\boldsymbol{\varepsilon}_{562} = 27.9\ mM^{-1}\ cm^{-1}$).

Measurement of dissociation constants (K_d) by Surface Plasmon Resonance (SPR).

SPR experiments were performed at 25 °C using a Biacore X100 instrument (GE Healthcare, Chicago, IL, USA) and a previously reported protocol[16]. In brief: Ab Bfr was immobilized on CM5 sensor chips (Cytiva, Marlborough, MA, USA) using amine coupling chemistry. The sensor surface was conditioned with 50 mM NaOH, 10 mM HCl, 0.1% SDS, and 0.085% (*w*/*v*) H_3PO_4, and then activated with 0.1 M N-hydroxysuccinimide (NHS) and 0.5 M N-ethyl-N'-3-(dimethylaminopropyl)carbodiimide hydrochloride (EDC) in water. The immobilization of Ab Bfr at the activated surface was performed by flowing (5 µL/min, 900 s) a solution of 100 nM Ab Bfr in 10 mM sodium acetate buffer (pH 4.5). The immobilization level was about 15,000 RU. Activated sites not bound to Ab Bfr were quenched by flowing (5 µL/min for 420 s) 1.0 M aqueous ethanolamine-HCl (pH 8.5). A flow cell activated by EDC/NHS and quenched by ethanolamine was used as the reference surface. To measure K_d values, a series of solutions of tagged-Bfd in SPR buffer (PBS pH 7.4 with 1 mM TCEP) was continually passed (5 µL/min) over the cell with immobilized Ab Bfr, allowing for 120 s contact time and 120 s dissociation time. K_d was evaluated as described in the Biacore Evaluation Software Handbook using Eq. 2, where R_{eq} is the SPR response at the plateau when the system reaches steady state equilibrium, R_{max} is the theoretical binding capacity, $[Bfd_f]$ is the concentration of Bfd passed over immobilized Ab Bfr, and *n*, which is the steric interference factor specifying the number of binding sites in Ab Bfr blocked by binding one analyte molecule (Bfd), was set to 0.91.

$$R_{eq} = R_{max}\left[Bfd_f\right] / \left(K_d + n\left[Bfd_f\right]\right) \tag{2}$$

Mobilization of iron from Ab Bfr

These experiments were carried out in an anaerobic chamber (Coy Lab Products) according to a previously reported method with modification[18]. Briefly, a 1 cm path-length cuvette was filled with a solution containing the Ab Bfr-tagged Bfd complex (0.38 µM), pa Fpr (7.7 µM) and α,α'-bipyridine (bipy) (2 mM). Iron mobilization was initiated by adding excess (1.5 mM) NADPH and monitored by following the intensity of the peak at 523 nm which corresponds to the formation of the $[Fe(bipy)_3]^{2+}$ complex.

Data availability

All data generated or analyzed in this study are included in this published article and its supplementary information files. The nucleotide sequence of Ab Bfd (locus Tag: A1S_3174) and Ab Bfr subunits Bfr (Locus Tag A1S_3175) and Ftn (Locus Tag A1S_0800) can be accessed at https://www.ncbi.nlm.nih.gov/nuccore/1263855999. Coordinates and structure factors for the Ab Bfr-Ftn heteropolymeric structure have been deposited to the Worldwide Protein Databank (https://www.rcsb.org/) with the accession code 9BTS.

Received: 29 May 2024; Accepted: 1 August 2024
Published online: 06 August 2024

References

1. Andrews, S. C. Iron storage in bacteria. *Adv. Microbial. Physiol.* **40**, 281–351 (1998).
2. Lundin, D., Poole, A. M., Sjoberg, B. M. & Hogbom, M. Use of structural phylogenetic networks for classification of the ferritin-like superfamily. *J. Biol. Chem.* **287**(24), 20565–20575. https://doi.org/10.1074/jbc.M112.367458 (2012).
3. Ruvinsky, A. M., Vakser, I. A. & Rivera, M. Local packing modulates diversity of iron pathways and cooperative behavior in eukaryotic and prokaryotic ferritins. *J. Chem. Phys.* **140**(11), 115104. https://doi.org/10.1063/1.4868229 (2014).
4. Rivera, M. Bacterioferritin: Structure, dynamics and protein-protein interactions at play in iron storage and mobilization. *Acc. Chem. Res.* **50**, 331–340. https://doi.org/10.1021/acs.accounts.6b00514 (2017).
5. Rivera, M. Mobilization of iron stored in bacterioferritin, a new target for perturbing iron homeostasis and developing antibacterial and antibiofilm molecules. *J. Inorg. Biochem.* **247**, 112306. https://doi.org/10.1016/j.jinorgbio.2023.112306 (2023).
6. Uebe, R. *et al.* Bacterioferritin of magnetospirillum gryphiswaldense is a heterotetraeicosameric complex composed of functionally distinct subunits but is not involved in magnetite biomineralization. *mBio* https://doi.org/10.1128/mBio.02795-18 (2019).

7. Bertani, L. E., Huang, J. S., Weir, B. A. & Kirschvink, J. L. Evidence for two types of subunits in the bacterioferritin of Magnetospirillum magnetotacticum. *Gene* **201**(1–2), 31–36. https://doi.org/10.1016/s0378-1119(97)00424-1 (1997).
8. Chen, C. Y. & Morse, S. A. Neisseria gonorrhoeae bacterioferritin: Structural heterogeneity, involvement in iron storage and protection against oxidative stress. *Microbiology* **145**(Pt 10), 2967–2975 (1999).
9. Weeratunga, S. *et al.* Structural Studies of Bacterioferritin B (BfrB) from *Pseudomonas aeruginosa* Suggest a Gating Mechanism for Iron Uptake via the Ferroxidase Center. *Biochemistry* **49**, 1160–1175. https://doi.org/10.1021/bi9015204 (2010).
10. Yao, H. *et al.* Two disctinct ferritin-like molecules in *P. aeruginosa*: The product of the bfrA gene is a bacterial ferritin (FtnA) not a bacterioferritin (Bfr). *Biochemistry* **50**, 5236–5248. https://doi.org/10.1021/bi2004119 (2011).
11. Bradley, J. M. *et al.* The ferroxidase centre of *Escherichia coli* bacterioferritin plays a key role in the reductive mobilisation of the mineral iron core. *Angew. Chem. Int. Ed. Engl.* **63**(16), e202401379. https://doi.org/10.1002/anie.202401379 (2024).
12. Eshelman, K. *et al.* Inhibiting the BfrB: Bfd interaction in pseudomonas aeruginosa causes irreversible iron accumulation in bacterioferritin and iron deficiency in the bacterial Cell. *Metallomics* **9**, 646–659. https://doi.org/10.1039/C7MT00042A (2017).
13. Bradley, J. M., Le Brun, N. E. & Moore, G. R. Ferritins: Furnishing proteins with iron. *J. Biol. Inorg. Chem.* **21**(1), 13–28. https://doi.org/10.1007/s00775-016-1336-0 (2016).
14. Abdul-Tehrani, H. *et al.* Ferritin mutants of Escherichia coli are iron deficient and growth impaired, and fur mutants are iron deficient. *J. Bacteriol.* **181**(5), 1415–1428 (1999).
15. Velayudhan, J., Castor, M., Richardson, A., Main-Hester, K. L. & Fang, F. C. The role of ferritins in the physiology of *Salmonella enterica* sv. Typhimurium: A unique role for ferritin B in iron-sulphur cluster repair and virulence. *Mol. Microbiol.* **63**(5), 1495–507. https://doi.org/10.1111/j.1365-2958.2007.05600.x (2007).
16. Yao, H. *et al. Pseudomonas aeruginosa* bacterioferritin is assembled from FtnA and BfrB subunits with the relative proportions dependent on the environmental oxygen availability. *Biomolecules* **12**(3), 366. https://doi.org/10.3390/biom12030366 (2022).
17. Yao, H. *et al.* The structure of the BfrB-Bfd complex reveals protein-protein interactions enabling iron release from bacterioferritin. *J. Am. Chem. Soc.* **134**(32), 13470–13481. https://doi.org/10.1021/ja305180n (2012).
18. Weeratunga, S. *et al.* Binding of *Pseudomonas aeruginosa* Apobacterioferritin-associated ferredoxin to bacterioferritin B promotes heme mediation of electron delivery and mobilization of core mineral iron. *Biochemistry* **48**, 7420–7431. https://doi.org/10.1021/bi900561a (2009).
19. Wang, Y. *et al.* Characterization of the bacterioferritin/bacterioferritin associated ferredoxin protein–protein interactions in solution and determination of binding energy hot spots. *Biochemistry* **54**, 6162–6175. https://doi.org/10.1021/acs.biochem.5b00937 (2015).
20. Punchi Hewage, A. N. D. *et al.* Mobilization of iron stored in bacterioferritin is required for metabolic homeostasis in *Pseudomonas aeruginosa*. *Pathogens* **9**(12), 980. https://doi.org/10.3390/pathogens9120980 (2020).
21. Soldano, A., Yao, H., Chandler, J. R. & Rivera, M. Inhibiting iron mobilization from bacterioferritin in *Pseudomonas aeruginosa* impairs biofilm formation irrespective of environmental iron availability. *ACS Infect. Dis.* **6**, 447–458. https://doi.org/10.1021/acsinfecdis.9b00398 (2020).
22. Punchi Hewage, A. N. D. *et al.* Small molecule inhibitors of the BfrB-Bfd interaction decrease *Pseudomonas aeruginosa* fitness and potentiate fluoroquinolone activity. *J. Am. Chem. Soc.* **141**(20), 8171–8184. https://doi.org/10.1021/jacs.9b00394 (2019).
23. Soldano, A. *et al.* Small molecule inhibitors of the bacterioferritin (BfrB)-ferredoxin (Bfd) complex kill biofilm-embedded *Pseudomonas aeruginosa* cells. *ACS Infect. Dis.* **7**(1), 123–140. https://doi.org/10.1021/acsinfecdis.0c00669 (2021).
24. Hempstead, P. D. *et al.* Comparison of the three-dimensional structures of recombinant human H and horse L ferritins at high resolution. *J. Mol. Biol.* **268**, 424–448 (1997).
25. Trikha, J., Theil, E. C. & Allewell, N. M. High resolution crystal structures of amphibian red cell L ferritin: Potential roles for structural plasticity and solvation in function. *J. Mol. Biol.* **248**, 949–967 (1995).
26. Wang, A. *et al.* Biochemical and structural characterization of *Pseudomonas aeruginosa* Bfd and FPR: Ferredoxin $NADP^+$ reductase and not ferredoxin is the redox partner of heme oxygenase under iron-starvation conditions. *Biochemistry* **46**, 12198–12211 (2007).
27. Wijerathne, H. *et al.* Bfd, a new class of [2Fe–2S] protein that functions in bacterial iron homeostasis, requires a structural anion binding site. *Biochemistry* **57**, 5533–5543. https://doi.org/10.1021/acs.biochem.8b00823 (2018).
28. Yariv, J. *et al.* The composition and structure of bacterioferritin of *Escherichia coli*. *Biochem. J.* **197**, 171–175 (1981).
29. Mohanty, A. *et al.* Alteration of coaxial heme ligands reveals the role of heme in bacterioferritin from *Mycobacterium tuberculosis*. *Inorg. Chem.* **60**(22), 16937–16952. https://doi.org/10.1021/acs.inorgchem.1c01554 (2021).
30. Hamburger, A. E., West, A. P. Jr., Hamburger, Z. A., Hamburger, P. & Bjorkman, P. J. Crystal structure of a secreted insect ferritin reveals a symmetrical arrangement of heavy and light chains. *J. Mol. Biol.* **349**(3), 558–569. https://doi.org/10.1016/j.jmb.2005.03.074 (2005).
31. Robinson, G. C. *et al.* Crystal structure of the pseudoenzyme PDX1.2 in complex with its cognate enzyme PDX1.3: A total eclipse. *Acta Crystallogr. D Struct. Biol.* **75**(Pt 4), 400–415. https://doi.org/10.1107/S2059798319002912 (2019).
32. Yao, H. *et al.* Concerted motions networking pores and distant ferroxidase centers enable bacterioferritin function and iron traffic. *Biochemistry* **54**(8), 1611–1627. https://doi.org/10.1021/bi501255r (2015).
33. Abramson, J. *et al.* Accurate structure prediction of biomolecular interactions with AlphaFold 3. *Nature* https://doi.org/10.1038/s41586-024-07487-w (2024).
34. P. AROSIO and S. LEVI: Structural and Functional Aspects. *Molecular and cellular iron transport*, 145 (2002)
35. British Medical Association. *Br. Med. J.* **2**(1197), 1113–1123 (1883).
36. Pereira, J. H., McAndrew, R. P., Tomaleri, G. P. & Adams, P. D. Berkeley Screen: A set of 96 solutions for general macromolecular crystallization. *J. Appl. Crystallogr.* **50**(Pt 5), 1352–1358. https://doi.org/10.1107/S1600576717011347 (2017).
37. Kabsch, W. Automatic indexing of rotation diffraction patterns. *J. Appl. Cryst.* **21**, 67–72. https://doi.org/10.1107/S0021889887700937 (1988).
38. Kabsch, W. Xds. *Acta Crystallogr. D Biol. Crystallogr.* **66**(Pt 2), 125–132. https://doi.org/10.1107/S0907444909047337 (2010).
39. Evans, P. R. An introduction to data reduction: Space-group determination, scaling and intentisy statistics. *Acta Cryst.* **D67**, 282–292. https://doi.org/10.1107/S090744491003982X (2011).
40. McCoy, A. J. *et al.* Phaser crystallographic software. *J. Appl. Cryst.* **40**, 658–674. https://doi.org/10.1107/S0021889807021206 (2007).
41. Afonine, P. V. *et al.* Towards automated crystallographic structure refinement with phenix.refine. *Acta Crystallogr. D Biol. Crystallogr.* **68**(4), 352–67. https://doi.org/10.1107/S0907444912001308 (2012).
42. Emsley, P., Lohkamp, B., Scott, W. G. & Cowan, K. Features and development of coot. *Acta Cryst.* **D66**, 486–501. https://doi.org/10.1107/S0907444910007493 (2010).
43. Potterton, L. *et al.* Developments in the CCP4 molecular-graphics project. *Acta Crystallogr. D Biol. Crystallogr.* **60**, 2288–2294 (2004).
44. Potterton, L. *et al.* Developments in the CCP4 molecular-graphics project. *Acta Crystallogr. D Biol. Crystallogr.* **60**(Pt 12 Pt 1), 2288–2294 (2004).
45. Krissinel, E. Enhanced fold recognition using efficient short fragment clustering. *J. Mol. Biochem.* **1**(2), 76–85 (2012).
46. Smith, M. G. *et al.* New insights into *Acinetobacter baumannii* pathogenesis revealed by high-density pyrosequencing and transposon mutagenesis. *Genes Dev.* **21**(5), 601–614. https://doi.org/10.1101/gad.1510307 (2007).
47. Ringeling, P. L. *et al.* Iron metabolism in *Rhodobacter capsulatus*. Characterisation of bacterioferritin and formation of non-haem iron particles in intact cells. *Eur. J. Biochem.* **223**(3), 847–55 (1994).

Acknowledgements
This research was funded by a grant from the National Institutes of Health (AI169344). The studies used resources at the NYX beamline 19-ID, supported by the New York Structural Biology Center, at the National Synchrotron Light Source II, a U.S. Department of Energy (DOE) Office of Science User Facility operated for the DOE Office of Science by Brookhaven National Laboratory under Contract No. DE-SC0012704. The NYX detector instrumentation was supported by grant S10OD030394 through the Office of the Director of the National Institutes of Health.

Author contributions
H.Y., A.S., and M.R. conceived the study. H.Y. purified native Ab Bfr, recombinant Ab Bfd and conducted the biochemical characterization. A.S. assisted with protein purification. S.A. purified recombinant Ab Bfr and conducted the iron titration experiments. L.F. performed mass spectrometry experiments. A.C. conducted all crystallization experiments and assisted with sample preparation and analysis. L.L. assisted with the structure refinement, K.P.B. performed the X-ray diffraction data collection and analysis, S.L. managed the structural biology tasks, conducted structure solution/refinement and manuscript preparation. D.V. made and analyzed multiple sequence alignments and AlphaFold 3.0 predicted structures. M.R. designed experiments, wrote the manuscript, and supervised the overall study. All authors reviewed and agreed with the contents of the manuscript.

Competing interests
The authors declare no competing interests.

Additional information
Supplementary Information The online version contains supplementary material available at https://doi.org/10.1038/s41598-024-69156-2.

Correspondence and requests for materials should be addressed to S.L. or M.R.